### Title

Will Anthropogenic Warming Increase Evapotranspiration? Examining Irrigation Water Demand Implications of Climate Change in California




### Journal

Earth's Future, 10(1)

### ISSN

2328-4277



### Authors

Vahmani, P
Jones, AD
Li, D



### Publication Date

2022

### DOI

10.1029/2021ef002221

Peer reviewed

Earth's Future

RESEARCH ARTICLE
10.1029/2021EF002221

# Will Anthropogenic Warming Increase Evapotranspiration? Examining Irrigation Water Demand Implications of Climate Change in California

**P. Vahmani[1], A. D. Jones[1], and D. Li[2]**

[1]Lawrence Berkeley National Laboratory, Berkeley, CA, USA, [2]Department of Earth and Environment, Boston University, Boston, MA, USA

**Key Points:**

- Increasing atmospheric temperature and vapor pressure deficit have minimal implications for evapotranspiration (ET) and irrigation water demand
- Regulation of stomata resistance by stressed vegetation offsets the expected increase in ET rates that would otherwise result from abiotic processes alone
- Anthropogenic warming of the atmosphere has minimal implications for mean relative humidity and the surface available energy, which are critical drivers of ET

**Supporting Information:**

Supporting Information may be found in the online version of this article.

**Correspondence to:**

P. Vahmani,
pvahmani@lbl.gov

**Citation:**

Vahmani, P., Jones, A. D., & Li, D. (2022). Will anthropogenic warming increase evapotranspiration? Examining irrigation water demand implications of climate change in California. *Earth's Future*, *10*, e2021EF002221. https://doi.org/10.1029/2021EF002221

Received 21 MAY 2021
Accepted 14 OCT 2021



**Abstract** Climate modeling studies and observations do not fully agree on the implications of anthropogenic warming for evapotranspiration (ET), a major component of the water cycle and driver of irrigation water demand. Here, we use California as a testbed to assess the ET impacts of changing atmospheric conditions induced by climate change on irrigated systems. Our analysis of irrigated agricultural and urban regions shows that warmer atmospheric temperatures have minimal implications for ET rates and irrigation water demands—about one percent change per degree Celsius warming (~1% $°C^{-1}$). By explicitly modeling irrigation, we control for the confounding effect of climate-driven soil moisture changes and directly estimate water demand implications. Our attribution analysis of the drivers of ET response to global anthropogenic warming shows that as the atmospheric temperature and vapor pressure deficit depart from the ideal conditions for transpiration, regulation of stomata resistance by stressed vegetation almost completely offsets the expected increase in ET rates that would otherwise result from abiotic processes alone. We further show that anthropogenic warming of the atmosphere has minimal implications for mean relative humidity (<1.7% $°C^{-1}$) and the surface available energy (<0.2% $°C^{-1}$), which are critical drivers of ET. This study corroborates the growing evidence that plant physiological changes moderate the degree to which changes in potential ET are realized as actual ET.

**Plain Language Summary** Climate modeling studies and observations do not fully agree on the implications of climate change-induced warming of the atmosphere for evapotranspiration (ET), a primary driver of irrigation water demand, despite its scientific and societal importance. Here, we use California as a testbed where we focus on vast irrigated urban and agricultural areas to assess the impacts of the warming climate on ET and irrigation water demand. Our analysis shows that warmer atmospheric temperatures have minimal implications for ET rates and irrigation water demand. We show that as the atmospheric temperature and humidity depart from the ideal conditions for transpiration, regulation of stomata resistance by stressed vegetation limits the increases in ET rates that would otherwise result from the increasing demand for moisture in the warmer atmosphere.

## 1. Introduction

Irrigation is the leading source of water demand in many of the world's water-scarce regions (Brauman et al., 2016). Therefore, understanding the implications of climate change for future irrigation water demand is of critical importance as any increase in water demand could further stress already constrained water delivery systems. A vast body of literature has established a significant correlation between climatic conditions and irrigation water demand and warned that implications of climate change for precipitation, temperature, relative humidity, wind speed, etc. can lead to an increased irrigation water demand across the globe (see a review by Wang et al. (2016)). However, there is little consensus on the magnitude of the predicted climate-induced increases in irrigation water demand. Ashour and Al-Najar (2013) predicted a range of 3–7% increases in irrigation water demand on the Gaza Strip due to increasing temperatures of 1–2 °C. Rodriguez Diaz et al. (2007) and de Silva et al. (2007) predicted climate-induced increases of 15%–20% and 13%–23% in irrigation needs by the 2050s in Spain and Sri Lanka, respectively. Generally, previous studies use an offline interpretation of climate model outputs along with the Penman-Monteith equation and water balance models to assess climate change impacts on irrigation demand. This approach does not allow these studies to explicitly address irrigation water demand over irrigated areas as irrigation is not represented in the majority of climate models (e.g., CMIP5). It also does not decompose dynamic

representation of plant physiological components, particularly stomatal resistance and its response to climate change-induced changes in atmospheric temperature, vapor pressure deficit, or $CO_2$ concentrations.

The primary driver of irrigation water demand is evapotranspiration (ET). Despite its scientific and societal importance, the implication of climate change for ET and associated irrigation water demands remains uncertain, as ET is influenced by a complex array of drivers and constraints ranging from global atmospheric processes to biotic leaf-scale processes, each of which is affected by climate change to varying degrees (Katul et al., 2012). Principle among these climate-sensitive drivers is atmosphere demand in the form of vapor pressure deficit (VPD), the effect of which is modulated by wind speed and available surface radiation. ET is also limited by available soil moisture and is regulated by plant physiology through changes in leaf stomatal conductance, which is known to respond to varying degrees to soil moisture, temperature, VPD, and atmospheric concentration of carbon dioxide ($CO_2$) (Katul et al., 2012).

Based on both theory and climate modeling studies, rising temperatures are expected to accelerate the global water cycle, resulting in increases in both precipitation and ET (Allen & Ingram, 2002; Huntington, 2006; Kunkel et al., 2013). In particular, under constant relative humidity, VPD and therefore atmospheric demand for ET are expected to track the Clausius-Clapeyron relationship, leading to ~6.8% global increase in these quantities per degree Celsius of warming (Allen & Ingram, 2002; Katul et al., 2012; Roderick et al., 2015). Several global modeling studies project slight decreases in relative humidity over continental interiors (Fu & Feng, 2014), which would lead to even greater increases in VPD and potential ET. However, the actual precipitation and ET increases estimated by global climate models are typically much smaller than that predicted by the Clausius-Clapeyron relationship (Allen & Ingram, 2002; Katul et al., 2012; Roderick et al., 2015).

The interpretation of climate model projections as implying that "warmer is more arid" based on projected increases in potential ET is in direct contrast with paleoclimate studies and observations of 20th century actual pan evaporation rates that imply "warmer is less arid," a dichotomy that has been termed the "global aridity paradox" (Roderick et al., 2015). Decreasing pan evaporation rates have been observed over the conterminous U.S. and Russia (Peterson et al., 1995), India, Venezuela, China, Australia, Thailand (Brutsaert, 2006), and there is evidence that global ET rates have declined during the first decade of the twenty-first century (Jung et al., 2010; Miralles et al., 2014; Wang et al., 2010). Various studies attribute the decreases in regional and global ET since the 1960s to changes in precipitation patterns and rates, diurnal air temperature ranges, aerosol concentrations, atmospheric vapor pressure deficit, and wind patterns (Douville et al., 2013; Hartmann et al., 2013; Pan et al., 2015; Romero-Lankao et al., 2014). Moreover, Roderick et al. (2015) demonstrate that since actual ET projected by global climate models is lower than projected potential ET, their results can be interpreted as more consistent with the observational record implying that "warmer is less arid."

One key to understanding lower projections of actual ET compared to VPD and potential ET is the role of plant stomatal conductance changes (Katul et al., 2012; Roderick et al., 2015). A recent body of literature has linked the aridity paradox to vegetation responses to rising atmospheric $CO_2$ concentrations (Kirschbaum & McMillan, 2018; Milly and Dunne, 2017; Roderick et al., 2015; Swann et al., 2016; Yang et al., 2019), although stomatal conductance also responds to changes in soil moisture, temperature, and VPD (Katul et al., 2012). These studies support the notion that climate change has two opposing implications for ET rates: the physical implication of rising temperature and vapor pressure deficit increases ET, while stomatal closure, particularly under elevated $CO_2$ concentrations, acts as a restraint on ET. However, most of these efforts rely on offline interpretations of climate model outputs (e.g., CMIP5 models) in a manner that does not decompose influences from radiative, aerodynamic components, and plant physiological components.

Understanding the implications of global climate models' ET results for irrigation water demand adds one more layer of complexity. On one hand, irrigated systems are simpler than natural ecosystems in that they are intentionally maintained with adequate soil moisture for plant growth, eliminating variability in a key factor that constrains ET. However, the global climate simulations that most of the above literature is based on do not typically represent irrigation. This makes it more difficult for the climate modeling studies to control for soil moisture availability when interpreting results, which is required to explicitly isolate the ET impacts of changing atmospheric conditions induced by climate change on irrigated systems.

Despite its drought-prone climate, California is a leading contributor to agricultural activity in the United States and home to the greatest share of the nation's population, 95% of which lives in highly irrigated urban areas

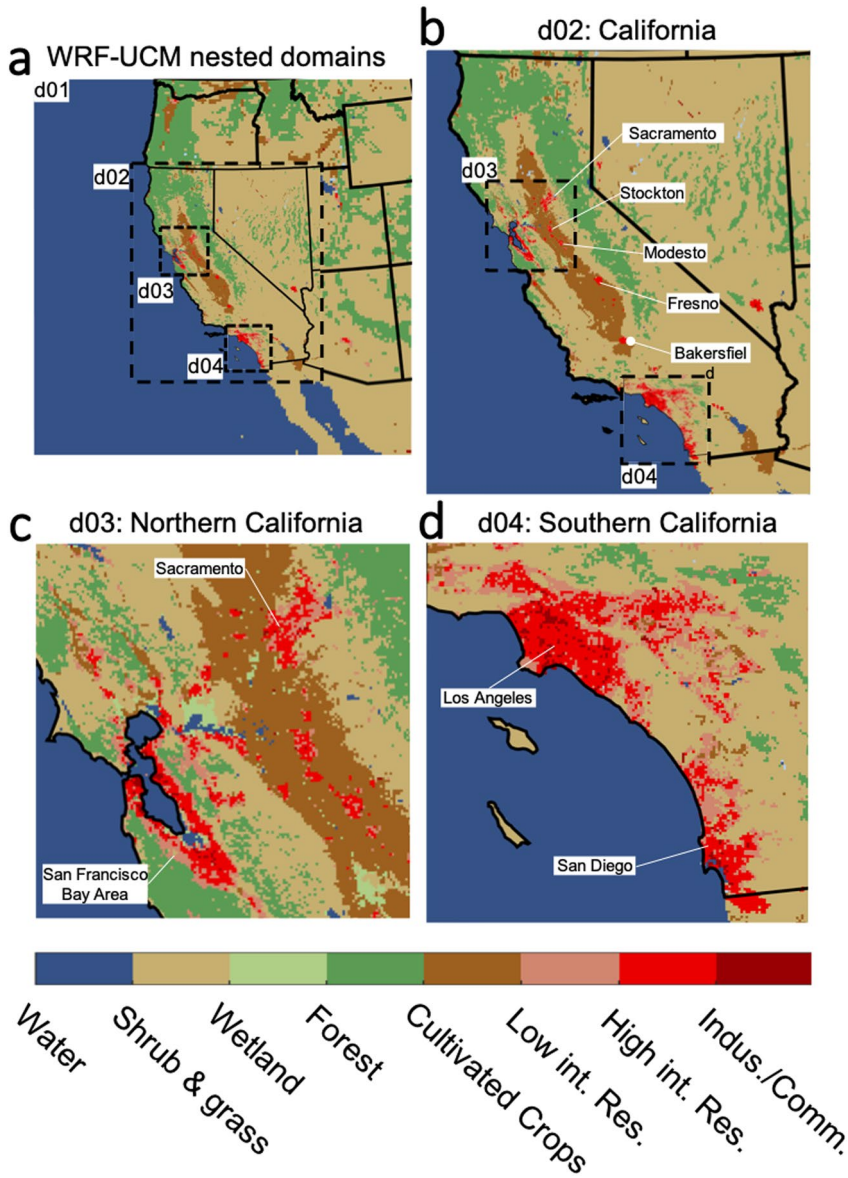


**Figure 1.** WRF-UCM domains, d01, d02, d03, and d04, with resolutions of 13.5, 4.5, 1.5, and 1.5 km, respectively (a); domain d02 (b); domain d03 (c); and domain d04 (d). Cultivated crops represent agricultural regions. Urban land classes include low-density residential (low int. res.), high-density residential (high int. res.), and industrial/commercial (indus./comm.).

(US Census Bureau, 2014) where irrigation can account for >50% of the municipal water consumption (Litvak et al., 2017). The competing water demands from different sectors (e.g., agriculture, urban, and industry) have historically resulted in the over-allocation of watersheds in the state (California Department of Water Resources, 1998). In addition to the climate change effects on the state's water supply (Hidalgo et al., 2009), it is critical to understand the implications of climate change for ET and irrigation water demands to ensure that the balance of water supply and demand levels in California can be maintained within a sustainable range (Kiparsky & Gleick, 2003; Milly et al., 2008).

In this study, we explicitly quantify the impacts of rising atmospheric temperatures on nonwater limited ET and irrigation water demands in agricultural and urban areas across California (Figure 1). We use a well-established regional climate model (WRF), coupled to an urban canopy model (UCM), high-resolution remote sensing of the land surface, and realistic urban and agricultural irrigation schemes that incorporate plant physiological

responses to temperature and VPD changes. We first simulate the summer irrigation season (June-October) for 15 historical years (2001–2015), then use a climate downscaling method (see Section 2) that modifies the historical conditions by imposing the midcentury regional warming signal derived from two CMIP5 models (CNRM-CM5 and HadGEM2-ES) and two Representative Concentration Pathways 4.5 and 8.5 (RCP4.5 and RCP8.5), which together span the possible temperature change range for California that could be reasonably expected, bound by a "warm" and a "hot" scenario. Our analysis focuses primarily on irrigated urban and agricultural areas, although we include values for nonirrigated lands for comparison as appropriate. Focusing on nonwater limited areas enables us to isolate the role of atmospheric and vegetation response, as opposed to soil moisture and water availability changes, and explicitly quantify irrigation demand implications.

## 2. Materials and Methods

### 2.1. WRF-UCM Configuration

We use WRF (version 3.6.1; Skamarock & Klemp, 2008; Skamarock et al., 2008), a well-established mesoscale numerical weather prediction model. To resolve urban canopy processes, WRF is coupled with a UCM (Kusaka & Kimura, 2004; Kusaka et al., 2001). The UCM accounts for shadowing, reflections, trapping of radiation, and wind profile within urban canyons, that reflect the three-dimensional nature of urban land and unique physical characteristics of built surfaces (Chen et al., 2011).

The parametrizations that represent physical processes in our WRF-UCM modeling framework include the Morrison double-moment scheme (Morrison et al., 2009) for microphysics, the Dudhia scheme (Dudhia, 1989) Rapid Radiative Transfer Model (Mlawer et al., 1997) for shortwave and longwave radiation, respectively, University of Washington (TKE) Boundary Layer Scheme (Bretherton & Park, 2009) for the planetary boundary layer, Grell-Freitas scheme (Grell & Freitas, 2014) for cumulus parameterization (used for domains d01 and d02 only), and the Eta Similarity scheme (Monin & Obukhov, 1954) for the surface layer.

We use the National Land Cover Data (NLCD; Fry et al., 2012) for a high-resolution (30 m) representation of urban and agricultural lands. We further incorporate in WRF-UCM, the high-resolution (30 m) NLCD impervious surface data (Wickham et al., 2013) to define impervious (or urban) fraction, independently (from land use/land cover). We further use the National Urban Database and Access Portal Tool (Ching et al., 2009) data set, where it is available, for a domain-specific representation of urban morphological parameters (i.e., building height, road width, etc.) in our WRF-UCM modeling framework.

Due to the importance of sea-surface temperature (SST) to the dynamics of regional and local climate along the California coast, we use a daily SST product (RTG_SST), by the National Centers for Environmental Prediction/Marine Modeling and Analysis Branch (NCEP/MMAB) in our simulations.

### 2.2. MODIS-Based Representation of Land Surfaces in WRF-UCM

Previous regional climate studies (Vahmani & Ban-Weiss, 2016) report that WRF-UCM performance can be improved by replacing the default climatological and tabulated representations of land surface physical characteristics with real-time high-resolution satellite-based representations of green vegetation fraction (GVF), albedo, and leaf area index (LAI). Here, we incorporate MODIS-based (2001–2015) monthly maps of GVF, albedo, and LAI based on MODIS vegetation indices (MOD13A3), reflectance (MCD43A3), and fraction of photosynthetically active radiation (MCD15A3) products, respectively. We reproject and regrid the MODID data to match our four WRF-UCM grids (d01, d02, d03, and d04). For more details on the incorporation of remote sensing data in WRF-UCM, see a previous study by the authors (Vahmani & Jones, 2017).

### 2.3. Study Domain

We configure WRF-UCM over four two-way nested domains illustrated in Figure 1. We focus our analysis on domains d02, d03, and d04. Domain d02, with a resolution of 4.5 km, engulfs the entire Central Valley which is a flat valley that stretches for 450 miles along with the interior of the state and holds one of the most important agricultural regions in the United States (Figure 1b). Domains d03 and d04, with a resolution of 1.5 km, cover

major urban areas in Northern and Southern California, respectively, including San Francisco Bay Area, Sacramento, Los Angeles, and San Diego (Figures 1c and 1d).

### 2.4. Simulation Design

We conduct three sets of WRF-UCM simulations to represent the implications of climate change for the drivers of ET and irrigation water demands across urban and agricultural lands in California: one Control scenario and two midcentury climate scenarios: "hot" and "warm." "Hot" and "warm" scenarios are driven by (a) the HadGEM2-ES GCM and RCP8.5 and (b) CNRM-CM5 GCM and RCP4.5, to represent the warmest and coolest midcentury California climate states, respectively. HadGEM2-ES and CNRM-CM5 are identified as the "warm" and "cool" models, respectively, by California's Fourth Climate Change Assessment (Pierce et al., 2016) from the 10 GCMs that most accurately reproduce California's climate. These two models along with RCP8.5 and RCP4.5 span the possible temperature change range for California that could be reasonably expected. For each scenario, we conduct 15 years of WRF-UCM simulations (2001–2015). Our analysis focuses on the growth/irrigation months of June-October. The Control scenario represents the current climate where the boundary and initial conditions are defined based on the North American Regional Reanalysis (NARR) data set (Mesinger et al., 2006). The climate change scenarios are designed based on a downscaling approach, described below.

Note that in reporting our results, we use the two-sided Student's *t*-test to evaluate the statistical significance of the changes relative to model internal variability and only report signals that are statistically significant with a 95% confidence level.

### 2.5. Downscaling Method (Climate Change)

Here, we follow a well-established downscaling approach (Pall et al., 2017; Patricola & Wehner, 2018; Rasmussen et al., 2011; Schär et al., 1996; Walton et al., 2015), referred to as "pseudo-global warming" or "delta" method, where a perturbation reflecting climate change signal is introduced to the initial and boundary conditions of the historical climate. The perturbations are calculated, for (a) HadGEM2-ES GCM and RCP8.5 ("hot" scenario) and (b) CNRM-CM5 GCM and RCP4.5 ("warm" scenario), as the differences between monthly climatology of the midcentury (2035–2064) and the historical period (1993–2022). The perturbations are calculated and applied for surface and near-surface air temperatures, air pressure, humidity, wind, sea-surface temperature, and geopotential height. This delta approach reduces the potential impacts of climate models' biases on WRF-UCM results, compared to the "direct downscaling" method where the boundary and initial conditions are derived from GCMs, directly. This approach further allows us to control the boundary conditions that we perturb in the climate change simulations. For this study, do not change soil moisture to control for water availability and assess the implications of atmospheric states only, for ET and irrigation water demands. For the climate change scenarios, we further modified greenhouse gases (GHG) concentrations in WRF, reflecting the radiative forcing of the corresponding RCP scenarios.

### 2.6. Irrigation Schemes

To represent irrigation and simulate the implications of climate change for irrigation water demand, we incorporate two irrigation schemes, for urban and agricultural irrigation, into the land surface model in the WRF-UCM modeling framework.

Over urban areas, we use a previously developed and validated (Vahmani & Hogue, 2014, 2015) urban irrigation scheme. This irrigation scheme accounts for irrigation of urban landscapes which is widespread in arid and semiarid regions such as California to maintain often nonnative urban vegetation. The urban irrigation scheme used here is based on a moisture deficit function, where irrigation water is applied on a predetermined interval to the pervious (or vegetated) portion of urban grid cells. During irrigation events, the moisture content of the topsoil layer is adjusted to the reference volumetric soil moisture content below which vegetation starts to stress. This irrigation scheme is designed to mimic common urban irrigation practices in that it occurs at a set interval. In our simulations, urban irrigation events happen three times per week, recommended and tested by previous studies in the region (Vahmani & Hogue, 2014, 2015). Note that the current irrigation scheme mimics an efficient irrigation system that avoids overirrigation or surface runoff by monitoring soil moisture to trigger and stop irrigation.

Over agricultural areas, we use a well-established (Ozdogan et al., 2010; Qian et al., 2013; Yang et al., 2017) irrigation scheme that has been implemented and validated over the California Central Valley (Yang et al., 2017). This irrigation scheme uses a green vegetation fraction (GVF) threshold and a soil moisture condition to trigger irrigation over agricultural (cultivated crops) areas, which are mapped based on a high-resolution (30 m) NLCD data set. Irrigation is triggered when real-time MODIS-based (see above) GVF exceeds a certain GVF threshold (Yang et al., 2017), indicating the agricultural grid cell is in the growing season, given by

$$\mathrm{GVF_{threshold}} = \mathrm{GVF_{min}} + 0.4 \times (\mathrm{GVF_{max}} - \mathrm{GVF_{min}}) \tag{1}$$

where $\mathrm{GVF_{max}}$ and $\mathrm{GVF_{min}}$ are the MODIS-based annual maximum and minimum green vegetation fraction at an agricultural grid cell, respectively.

The soil moisture condition is defined based on a soil moisture availability factor ($\mathrm{SM_{available}}$) that reflects soil moisture availability in the crop root zone (Qian et al., 2013; Yang et al., 2017). $\mathrm{SM_{available}}$ is defined as the ratio of the difference between the soil moisture in the root zone (SM) and the wilting point ($\mathrm{SM_{WP}}$) and the difference between soil field capacity ($\mathrm{SM_{FC}}$) and $\mathrm{SM_{WP}}$, given by

$$\mathrm{SM_{available}} = \frac{\mathrm{SM\text{-}SM_{WP}}}{\mathrm{SM_{FC}\text{-}SM_{WP}}} \tag{2}$$

The soil moisture condition for irrigation is met when $\mathrm{SM_{available}}$ falls below the threshold of 43%, recommended for California Central Valley by previous studies in the region (see Yang et al., 2017). When and where the GVF threshold and soil moisture condition are met, an irrigation event is triggered to increase the soil moisture in the root zone to the field capacity ($\mathrm{SM_{FC}}$), which is the maximum amount of moisture soil can hold against gravity. Similar to urban irrigation, agricultural irrigation events occur after sunset to avoid heavy moisture losses under direct sun exposure.

### 2.7. Attribution of Change in ET

The Penman-Monteith equation calculates ET as

$$ET = \frac{sR_n + \rho_a C_P D/r_a}{s + \gamma\left(1 + \frac{r_s}{r_a}\right)} \tag{3}$$

where $R_n$ is available surface energy (i.e., net radiation at the surface minus ground heat flux), $s$ is the gradient of the saturation vapor pressure with respect to temperature, $\rho_a$ is mean air density at constant pressure, $C_P$ is the specific heat at constant pressure, and $\gamma$ is the psychrometric constant. $D$ is the near-surface vapor pressure deficit, $r_s$ is the bulk surface resistance, $r_a$ is the aerodynamic resistance, and $\lambda$ is the latent heat of vaporization.

According to the Penman-Monteith equation (Equation 3), five key variables are most responsible for changes in ET, that is, $R_n$, $D$, $r_s$, $r_a$, and $s$, given changes in $\lambda$ are generally small. Similar to the approach adopted in Yang et al. (2019), we approximate changes in ET ($\Delta$ET) as a function of its partial differentials with respect to these five variables and changes in these variables ($\Delta R_n, \Delta D, \Delta r_s, \Delta r_a$, and $\Delta s$) as:

$$\Delta ET \approx \frac{\partial ET}{\partial R_n}\Delta R_n + \frac{\partial ET}{\partial D}\Delta D + \frac{\partial ET}{\partial r_s}\Delta r_s + \frac{\partial ET}{\partial r_a}\Delta r_a + \frac{\partial ET}{\partial s}\Delta s \tag{4}$$

where

$$\frac{\partial ET}{\partial R_n} = \frac{s}{\lambda\left[s + \gamma\left[1 + \frac{r_s}{r_a}\right]\right]} \tag{5}$$

$$\frac{\partial ET}{\partial D} = \frac{\rho_a C_P}{\lambda r_a\left[s + \gamma\left[1 + \frac{r_s}{r_a}\right]\right]} \tag{6}$$

$$\frac{\partial ET}{\partial r_s} = \frac{-\gamma\left[sR_n + \frac{\rho_a C_P D}{r_a}\right]}{\lambda r_a\left[s + \gamma\left[1 + \frac{r_s}{r_a}\right]\right]^2} \tag{7}$$

$$\frac{\partial ET}{\partial r_a} = \frac{\gamma r_s\left[sR_n + \frac{\rho_a C_P D}{r_a}\right]}{\lambda {r_a}^2\left[s + \gamma\left[1 + \frac{r_s}{r_a}\right]\right]^2} - \frac{\rho_a C_P D}{\lambda {r_a}^2\left[s + \gamma\left[1 + \frac{r_s}{r_a}\right]\right]} \tag{8}$$

$$\frac{\partial ET}{\partial s} = \frac{R_n}{\lambda\left[s + \gamma\left[1 + \frac{r_s}{r_a}\right]\right]} - \frac{sR_n + \frac{\rho_a C_P D}{r_a}}{\lambda\left[s + \gamma\left[1 + \frac{r_s}{r_a}\right]\right]^2} \tag{9}$$

### 2.8. Model Validation

We validate the model performance against ground-based observations of near-surface air temperature and ET (Figures S6 and S7 in Supporting Information S1). We compare simulated daily mean and maximum air temperatures to observations, based on 64 ground stations across California from the National Climatic Data Center (NCDC) network (Figure S6 in Supporting Information S1). This validation analysis shows that WRF-UCM reproduces the daily temperature variations with reasonable accuracy: RMSDs of 1.1 and 0.4 °C for daily mean and maximum air temperatures, respectively. We future use hourly estimates of reference ET (ET0) based on ground observations from California Irrigation Management Information System (CIMIS) stations in urban areas across California. CIMIS stations are designed to record hourly meteorological conditions over well-watered, closely clipped, actively growing grass fields. This information is then used to estimate hourly reference ET (http://www.cimis.water.ca.gov/Resources.aspx). Here, we compare WRF-UCM simulated ET, over urban landscapes (impervious or vegetated urban areas), to reference ET observations from 34 CIMIS stations (Figure S7 in Supporting Information S1). This analysis shows that the model estimates the measured reference ETs with reasonable accuracy: RSMD of 0.6 and 0.7 mm day$^{-1}$, for domains d03 and d04, respectively.

We note that we use the Penman-Monteith equation to diagnose the contribution of different relevant variables to ET changes, while the changes in ET are predicted by a more sophisticated land surface scheme in WRF-UCM. The resulting uncertainty in our attribution analysis is evaluated by comparing the attributed changes in ET, based on partial differentials of five terms ($R_n$, $D$, $r_a$, $r_s$, and $s$) in the Penman-Monteith equation (see Section 2.7), and the WRF-UCM simulated changes in ET. We find good agreement between attributed and modeled changes, as illustrated in Figure S8 in Supporting Information S1 (RMSE of 0.016 mm day$^{-1}$ and $R^2$ of 0.98). The remaining biases are related to the differences between the Penman-Monteith model and the scheme used in WRF-UCM calculation of ET and the exclusion of other terms in the Penman-Monteith equation (e.g., $\lambda$ or psychrometric constant) in the attribution analysis.

## 3. Results

Figure 2 shows that under "hot" midcentury climate, ET rates over agricultural and urban areas and averaged over 15 years, are increased by 3.3%, which is equivalent to about one percent change per degree Celsius warming (1.4% °C$^{-1}$), given the average warming of 2.3 °C (Figure S1 in Supporting Information S1). These results indicate an ET change rate that is much smaller than the anticipated global hydrologic cycle acceleration rate of ~6.8% °C$^{-1}$, due to the global warming temperatures, calculated based on the Clausius-Clapeyron equation (Katul et al., 2012). With small changes in ET, changes in irrigation water demand are also small: 2.6% (the equivalent of 1.1% °C$^{-1}$) under the "hot" scenario. Less significant absolute changes and a similar rate change (of ~1% °C$^{-1}$) are found under the "warm" scenario (Figure S2 in Supporting Information S1).

To understand the reasons that underpin limited ET response to warming atmospheric temperatures, we attribute midcentury ET changes to different forcing factors in the Penman-Monteith equation (see Section 2) that include surface available energy ($R_n$), vapor pressure deficit ($D$), aerodynamic resistance ($r_a$), surface resistance ($r_s$), and gradient of the saturation vapor pressure with respect to temperature ($s$). Under the "hot" scenario, our results

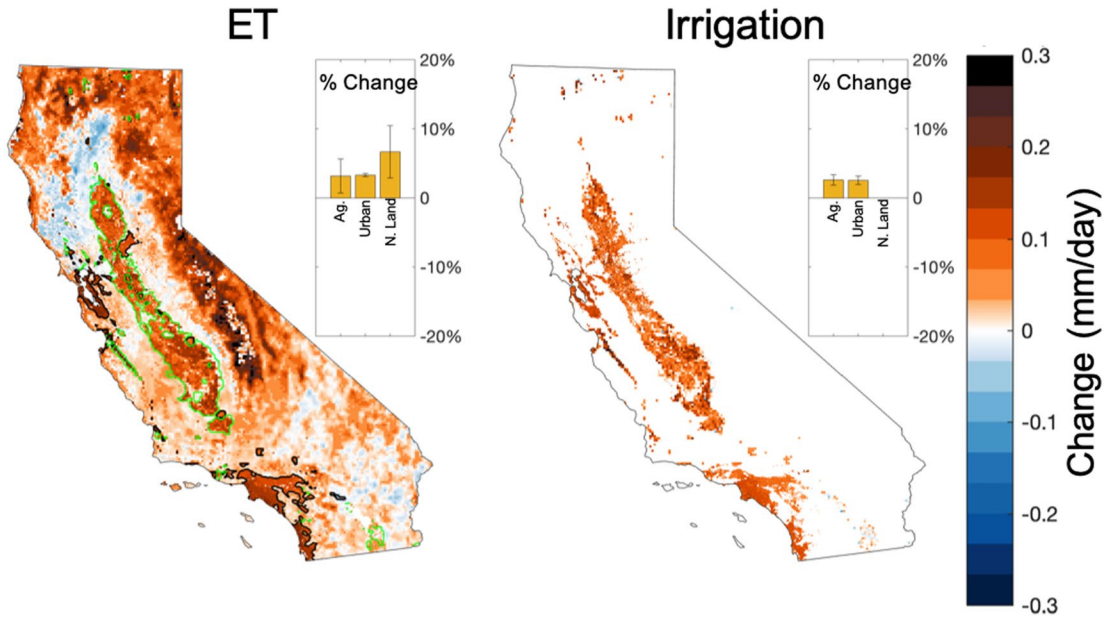


**Figure 2.** WRF-UCM simulated changes in evapotranspiration (ET) and irrigation water demand due to midcentury climate change under the "hot" scenario. See Figure S2 in Supporting Information S1 for the "warm" scenario. Values are 15-year daytime (6 a.m.–6 p.m.) averages in mm day$^{-1}$ over June-October. Green and black lines show the boundaries of agricultural and urban areas, respectively. Bar plots show averages over agricultural (Ag.), irrigated urban (Urban), and natural land (N. Land) grid cells. Values over urban areas represent the pervious or vegetation potions only. Note that only changes that are statistically distinguishable from zero at a 95% confidence interval are included.

(Figure 3a) show significant increases in $D$, $r_s$, and $s$ of 14%, 10%, and 12%, respectively, while changes in $R_n$ and $r_a$ are minimal. The increases in $D$, $r_s$, and $s$, in turn, lead to changes in ET of +7%, −6%, and +2%, adding to a total ET increase of ∼+3% (Figure 3b). A similar pattern is found under the "warm" scenario (Figure S3 in Supporting Information S1). These results indicate that as the temperature and vapor pressure deficit in the atmosphere depart from the ideal conditions for transpiration, the regulation of stomata resistance by stressed vegetation almost completely offsets the expected increase in ET rates that would otherwise result from abiotic processes alone. These findings further show that anthropogenic warming of the atmosphere has minimal implications for mean relative humidity (<1.7% °C$^{-1}$) and the surface available energy (<0.2% °C$^{-1}$), which are critical drivers of ET.

Note that the parameterization of $r_s$ in Noah LSM, incorporated in WRF, similar to many other land surface models, is based on minimum stomatal resistance ($Rc_{min}$), leaf area index (LAI), and four stress factors that represent the effects of vapor pressure deficit, solar radiation, soil moisture, and air temperature (Chen et al., 1996). Vegetation type and therefore $Rc_{min}$ and LAI are constant between current and future climate scenarios in our simulations. Note that we do not consider the potential vegetation response to elevated atmospheric $CO_2$ concentrations. Changes in incoming solar radiation are minimal and we control for soil moisture in our delta method (see Section 2) and by limiting our analysis to irrigated areas (see Figure S4 in Supporting Information S1) for change in soil moisture and precipitation). Hence, the reported changes in $r_s$ are solely due to stress factors driven by air temperature and vapor pressure deficit.

Monteith (1995) described that ET increases as $D$ increases up to an optimal $D$, after which it stabilizes and eventually decreases in very dry air because of the patchy closure of stomata. One interpretation of our results is that, on average, the summertime vapor pressure deficit in California is at or close to the optimal value and any further increase would result in minimal ET reaction due to regulation of stomata resistance. And, a continuation of drying of the atmosphere to extreme levels would result in decreasing ET rates. In the current study, we find a VPD change rate of 6.1% °C$^{-1}$, which is slightly lower than the rate indicated by the Clausius-Clapeyron relationship under constant relative humidity (6.8% °C$^{-1}$), which is expected as the mean temperature in our study domain (26.0 and 22.9 °C, over agricultural and urban areas, respectively) is higher than the global mean air temperature of 15 °C, assumed in the calculation of 6.8% °C$^{-1}$ acceleration rate (Kunkel et al., 2013). Although global climate

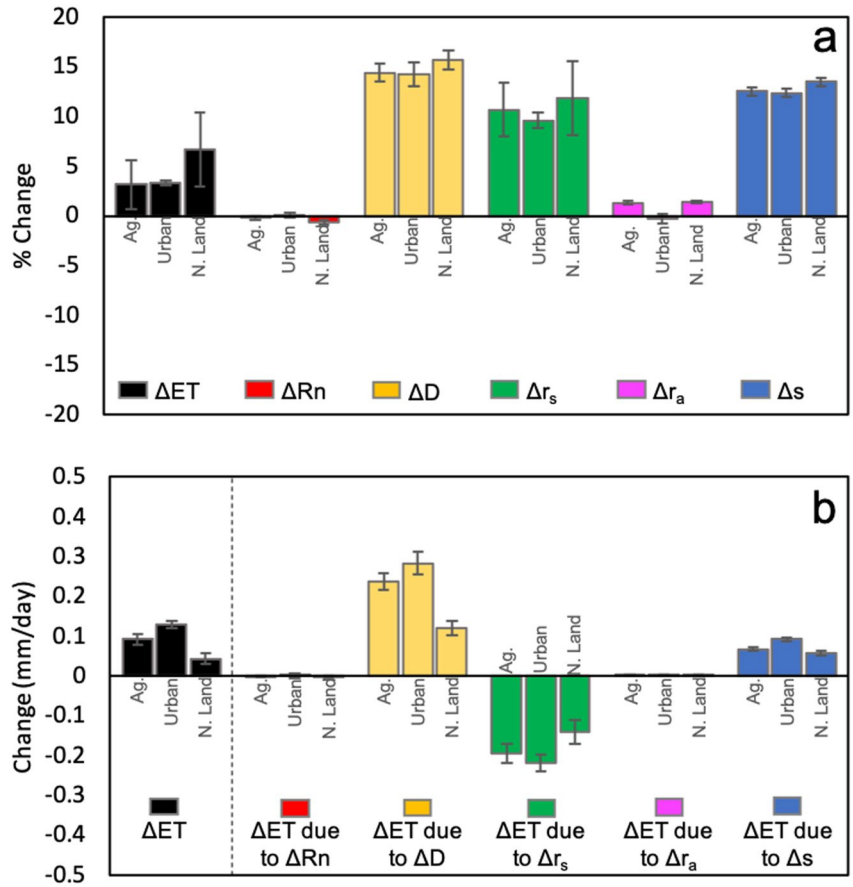


**Figure 3.** Climate change-induced changes in forcing factors in the Penman-Monteith equation: surface available energy ($R_n$), vapor pressure deficit ($D$), surface resistance ($r_s$), aerodynamic resistance ($r_a$), and gradient of the saturation vapor pressure with respect to temperature ($s$) (a) and attribution of changes in ET, induced by climate change, to these factors (b). The error bars illustrate the standard deviation of interannual fluctuations. The climate change scenario represents "hot" midcentury. See Figure S3 in Supporting Information S1 for the "warm" scenario. Values are 15-year averages over irrigated agricultural (Ag.), irrigated urban regions (Urban), and natural land (N. Land), daytime (6 a.m.–6 p.m.), and June-October. Values over urban areas are calculated for the pervious or vegetation potions. Note that only changes that are statistically distinguishable from zero at a 95% confidence interval are included.

change causes a significant change in the atmospheric temperatures (under the "hot" scenario) and consequently in saturation vapor pressure, specific humidity also increases. Increasing specific humidity dampens increases in vapor VPD and keeps relative humidity relatively constant, especially near the coast as has been observed to date (Hartmann et al., 2013; Trenberth et al., 2007; Figure 4). We further find more substantial increases in VPD extremes compared to overall seasonal mean VPD (see Figure S5 in Supporting Information S1) which could reach the tipping point described by Montheith (1995) and result in decreased ET rates, corroborating the findings of a recent observational study similarly showing that stomatal resistance can lead to decreases in ET during heatwave periods (Wang et al., 2019).

Our results are broadly consistent with recent findings by Yang et al. (2019), who found that increases in stomatal resistance lead to relatively minor implications for ET rates despite a warming-induced vapor pressure deficit increase. Yang et al. (2019) attribute increased stomatal resistance to elevated $CO_2$ concentrations. Interestingly, we show that indirect implications of higher $CO_2$ concentration, higher temperatures, and vapor pressure deficit, alone trigger a vegetation response that can entirely offset the $D$-induced changes in ET, without considering the vegetation reaction to a $CO_2$-enriched environment.

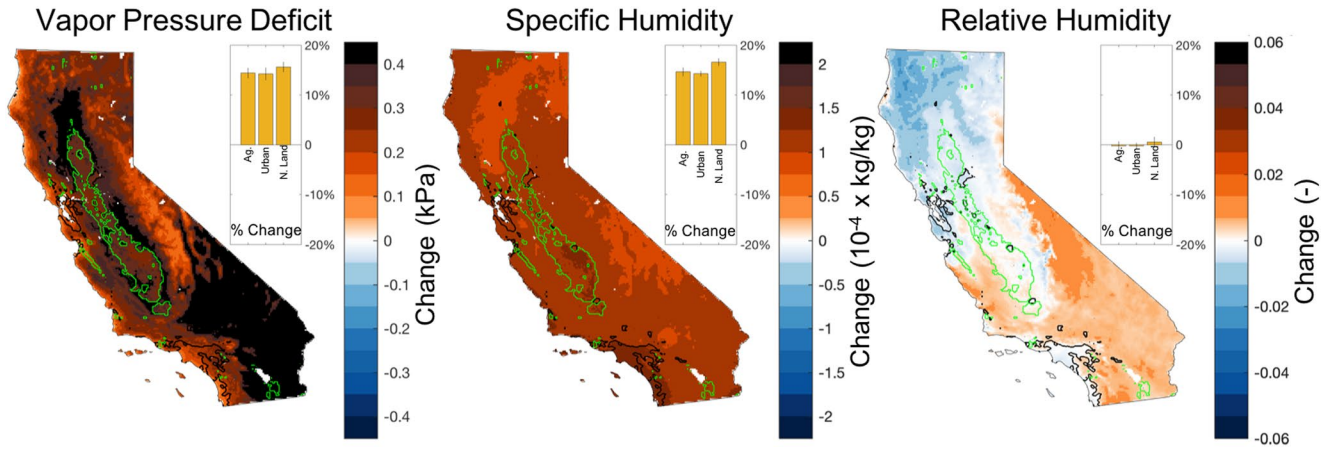


**Figure 4.** WRF-UCM simulated changes in vapor pressure deficit, specific humidity, and relative humidity due to midcentury climate change under the "hot" scenario. Values are 15-year daytime (6 a.m. – 6 p.m.) averages over June-October. Green and black lines show the boundaries of agricultural and urban areas, respectively. Bar plots show averages over agricultural land (Ag.), irrigated urban areas (Urban), and natural land (N. Land). Values over urban areas represent the pervious or vegetation potions only. Note that only changes that are statistically distinguishable from zero at a 95% confidence interval are included.

## 4. Conclusions

Here, we address the "global aridity paradox" with a case study of the implications of climate change for ET and irrigation water demand in irrigated agricultural and urban areas in California. Our results suggest that anthropogenic warming of the atmosphere and consequent elevated vapor pressure deficit have minimal implications for the future of ET rates and thereby for irrigation water demand. By controlling for water availability, we show that the warming temperatures, due to climate change, lead to ET and irrigation water demand increases of around 1% $°C^{-1}$. Consistent with Roderick et al. (2015) these findings refute the common interpretation of climate modeling results as suggesting that "warmer is more arid" or that elevated temperatures amplify ET and thereby drying rates. Rather, our results indicate that warmer is neither more nor less arid.

Our attribution analysis of the drivers of ET response to global anthropogenic warming shows that as the temperature and vapor pressure deficit in the atmosphere depart from the ideal conditions for transpiration, the regulation of stomata resistance by stressed vegetation almost completely offsets the expected increase in ET rates that would otherwise result from abiotic processes alone. We further show that anthropogenic warming of the atmosphere has minimal implications for mean relative humidity (<1.7% $°C^{-1}$) and the surface available energy (<0.2% $°C^{-1}$), which are the main drivers of ET. Overall, these findings refute the notions that warming climate and resultant rising evaporative demand will lead to significant drying and indeed show that ET rates remain relatively unchanged by the warmer midcentury atmospheric temperatures.

We note that we do not consider the potential vegetation response to elevated atmospheric $CO_2$ concentrations, in the form of further increases in stomata resistance. We speculate that this response to higher $CO_2$ concentrations, in addition to the response to increasing atmospheric temperatures and vapor pressure deficit, as illustrated in this study, could lead to a tipping point where ET rates are reduced, despite higher evaporative demand in the atmosphere as has been observed (Brutsaert, 2006; Jung et al., 2010; Miralles et al., 2014; Mueller et al., 2013; Peterson et al., 1995; Wang et al., 2010). On the other hand, we do not explicitly consider how cropping practices might change under a warmer climate. Longer growing seasons, an extended dry season with less precipitation in the fall, and the growth of more water-intensive crops that take advantage of greater water use efficiency under elevated $CO_2$ conditions could all increase irrigation water demand in our study region in ways beyond the scope of the current study. Furthermore, the implications of the warming atmosphere for ET reported here, should be verified over regions with climates vastly different from California.

We note that our findings are subject to several model-based and data-based uncertainties. There are uncertainties associated with atmospheric processes represented in WRF as well as the initial and boundary conditions. We recognize these uncertainties despite the fact that we use previously established parametrizations in WRF-UCM and evaluate the model performance against ground observations of air temperature and evapotranspiration

(Figures S6 and S7 in Supporting Information S1). Similarly, there are uncertainties associated with the parameterization of plant physiological processes in the WRF-UCM framework. We discuss this parameterization and calculation of surface resistance in Section 3, which involves estimates of minimum stomatal resistance, leaf area index, and stress factors that are subject to uncertainties in the representation of vegetation types in the model. Furthermore, the irrigation scheme, although based on previously validated and established methodology and evaluated against ground observations of ET, is subjected to uncertainties associated with factors related to human behavior, socioeconomics, and water pricing as well as representations of land use/cover, vegetation type, and soil type in the model. Finally, there are uncertainties associated with the attribution analysis used in this study. We note that the Penman-Monteith equation is used to diagnose the factors contributing to ET changes, while the changes in ET are predicted based on a more sophisticated land surface scheme in the WRF-UCM framework. The differences between the attributed changes in ET, based on partial differentials of variables in the Penman-Monteith equation, and the WRF-UCM-simulated changes in ET are evaluated in Section 2.8 (Figure S8 in Supporting Information S1).

In light of the growing evidence that plant physiological changes moderate the degree to which changes in potential ET are realized as actual ET, care should be taken in interpreting studies that examine climate change implications for water demand (Anderson et al., 2008; Ashour & Al-Najar, 2013; de Silva et al., 2007; Rodriguez Diaz et al., 2007; Wang et al., 2016), drought (AghaKouchak et al., 2014; Cook et al., 2015; Diffenbaugha et al., 2015; Griffin & Anchukaitis, 2014; Mann & Gleick, 2015; Shukla et al., 2015; Williams et al., 2015), or wildfire (Abatzoglou & Williams, 2016; Littell et al., 2009, 2016; Seager et al., 2015) using temperature-based metrics such as the Palmer Drought Severity Index or related metrics based on atmospheric moisture demand or potential ET. When considering plant responses directly to temperature and VPD changes, or $CO_2$ change over time, actual ET may be lower than indicated by such metrics.

We note, though, that this study solely focuses on the implications of anthropogenic warming of the atmosphere for ET rates and irrigation water demand, particularly in nonwater limited conditions. Climate change is still expected to impact water availability and drought and wildfire intensity and impact, e.g., through implications for precipitation patterns and variability, rainfall versus snow ratio, snowpack water storage, or evaporation from bare soil. Moreover, our finding that short-term extreme VPD conditions increase at a higher rate than the mean, maybe particularly important to consider in the context of wildfire management.

## Data Availability Statement

The WRF-UCM code, NARR, NLCD, and MODIS data, used in this study, are openly available. WRF-UCM simulations outputs are deposited in a repository at https://doi.org/10.5281/zenodo.5771142. The repository also includes a detailed description of WRF-UCM configuration, inputs, relevant namelist, and tables, along with scripts used to postprocess WRF-UCM data and create figures.

**Acknowledgments**
This research was supported by the U.S. Department of Energy, Office of Science, as part of research in the MultiSector Dynamics, Earth and Environmental System Modeling Program. This research used resources of the National Energy Research Scientific Computing Center (NERSC), a DOE Office of Science User Facility supported by the Office of Science of the U.S. Department of Energy under Contract No. DEAC02-05CH11231.

## References

Abatzoglou, J. T., & Williams, A. P. (2016). Impact of anthropogenic climate change on wildfire across western US forests. *Proceedings of the National Academy of Sciences of the United States of America*, *113*(42), 11770–11775. https://doi.org/10.1073/pnas.1607171113

AghaKouchak, A., Cheng, L., Mazdiyasni, O., & Farahmand, A. (2014). Global warming and changes in risk of concurrent climate extremes: Insights from the 2014 California drought. *Geophysical Research Letters*, *41*, 8847–8852. https://doi.org/10.1002/2014GL062308

Allen, M. R., & Ingram, W. J. (2002). Constraints on future changes in climate and the hydrologic cycle. *Nature*, *419*, 224–232. https://doi.org/10.1038/nature01092

Anderson, J., Chung, F., Anderson, M., Brekke, L., Easton, D., Ejeta, M., et al. (2008). Progress on incorporating climate change into management of California's water resources. *Climatic Change*, *87*, 91–108. https://doi.org/10.1007/s10584-007-9353-1

Ashour, E. K., & Al-Najar, A. (2013). The impact of climate change and soil salinity in irrigation water demand on the Gaza Strip. *Journal of Water and Climate Change*, *4*(2), 118–130.

Brauman, K. A., Richter, B. D., Postel, S., Malsy, M., & Florke, M. (2016). Water depletion: An improved metric for incorporating seasonal and dry-year water scarcity into water risk assessments. *Elementa: Science of the Anthropocene*, *4*, 000083. https://doi.org/10.12952/journal.elementa.000083

Bretherton, C. S., & Park, S. (2009). A new moist turbulence parameterization in the community atmosphere model. *Journal of Climate*, *22*, 3422–3448. https://doi.org/10.1175/2008jcli2556.1

Brutsaert, W. B. (2006). Indications of increasing land surface evaporation during the second half of the 20th century. *Geophysical Research Letters*, *33*, L20403. https://doi.org/10.1029/2006GL027532

California Department of Water Resources. (1998). *California water plan*. Updated Bulletin 160-98. California Department of Water Resources.

Chen, F., Kusaka, H., Bornstein, R., Ching, J., Grimmond, C. S. B., Grossman-Clarke, S., et al. (2011). The integrated WRF/urban modeling system: Development, evaluation, and applications to urban environmental problems. *International Journal of Climatology*, *31*, 273288. https://doi.org/10.1002/joc.2158

Chen, F., Mitchell, K., Schaake, J., Xue, Y., Pan, H.-L., Koren, V., et al. (1996). Modeling of land surface evaporation by four schemes and comparison with FIFE observations. *Journal of Geophysical Research*, *101*(D3), 7251–7268. https://doi.org/10.1029/95JD02165

Ching, J., Brown, M., Burian, S., Chen, F., Cionco, R., Hanna, A., et al. (2009). National urban database and access portal tool. *Bulletin of the American Meteorological Society*, *90*, 1157–1168. https://doi.org/10.1175/2009bams2675.1

Cook, B. I., Ault, T. R., & Smerdon, J. E. (2015). Unprecedented 21st century drought risk in the American Southwest and Central Plains. *Science Advances*, *1*(1), e1400082. https://doi.org/10.1126/sciadv.1400082

de Silva, C. S., Weatherhead, E. K., Knox, J. W., & Rodriguez-Diaz, J. A. (2007). Predicting the impacts of climate change—A case study of paddy irrigation water requirements in Sri Lanka. *Agricultural Water Management*, *93*(1), 19–29. https://doi.org/10.1016/j.agwat.2007.06.003

Diffenbaugha, N. S., Swaina, D. L., & Toumaa, D. (2015). Anthropogenic warming has increased drought risk in California. *Proceedings of the National Academy of Sciences of the United States of America*, *112*(13), 3931–3936. https://doi.org/10.1073/pnas.1422385112

Douville, H., Ribes, A., Decharme, B., Alkama, R., & Sheffield, J. (2013). Anthropogenic influence on multidecadal changes in reconstructed global evapotranspiration. *Nature Climate Change*, *3*, 59–62. https://doi.org/10.1038/nclimate1632

Dudhia, J. (1989). Numerical study of convection observed during the winter monsoon experiment using a mesoscale two dimensional model. *Journal of the Atmospheric Sciences*, *46*, 3077–3107. https://doi.org/10.1175/1520-0469(1989)046<3077:nsocod>2.0.co;2

Fry, J. A., Xian, G., Jin, S., Dewitz, J. A., Homer, C. G., Yang, L., & Barnes, C. A. (2012). Completion of the 2006 national land cover database update for the conterminous United States. *Photogrammetric Engineering & Remote Sensing*, *77*, 858–864.

Fu, Q., & Feng, S. (2014). Responses of terrestrial aridity to global warming. *Journal of Geophysical Research: Atmosphere*, *119*, 7863–7875. https://doi.org/10.1002/2014JD021608

Grell, G. A., & Freitas, S. R. (2014). A scale and aerosol aware stochastic convective parameterization for weather and air quality modeling. *Atmospheric Chemistry and Physics*, *14*, 5233–5250. https://doi.org/10.5194/acp-14-5233-2014

Griffin, D., & Anchukaitis, K. J. (2014). How unusual is the 2012–2014 California drought? *Geophysical Research Letters*, *41*, 9017–9023. https://doi.org/10.1002/2014GL062433

Hartmann, D. L., Klein Tank, A. M. G., Rusticucci, M., Alexander, L. V., Brönnimann, S., Charabi, Y., et al. (2013). Observations: Atmosphere and surface. In T. F. Stocker, D. Qin, G.-K. Plattner, M. Tignor, S. K. Allen, J. Boschung, et al. (Eds.), *Climate change 2013: The physical science basis. Contribution of working group I to the fifth assessment report of the intergovernmental panel on climate change* (pp. 159–254). Cambridge University Press. https://doi.org/10.1017/CBO9781107415324.008

Hidalgo, H. G., Das, T., Dettinger, M. D., Cayan, D. R., Pierce, D. W., Barnett, T. P., et al. (2009). Detection and attribution of streamflow timing changes to climate change in the western United States. *Journal of Climate*, *22*, 3838–3855. https://doi.org/10.1175/2009jcli2470.1

Huntington, T. G. (2006). Evidence for intensification of the global water cycle: Review and synthesis. *Journal of Hydrology*, *319*, 83–95. https://doi.org/10.1016/j.jhydrol.2005.07.003

Jung, M., Reichstein, M., Ciais, P., Seneviratne, S., Sheffield, J., Goulden, M. L., et al. (2010). Recent decline in global land evapotranspiration trend due to limited moisture supply. *Nature*, *467*, 951–954. https://doi.org/10.1038/nature09396

Katul, G. G., Oren, R., Manzoni, S., Higgins, C., & Parlange, M. B. (2012). Evapotranspiration: A process driving mass transport and energy exchange in the soil-plant-atmosphere-climate system. *Reviews of Geophysics*, *50*, RG3002. https://doi.org/10.1029/2011RG000366

Kiparsky, M., & Gleick, P. H. (2003). *Climate change and California water resources: A survey and summary of the literature (Report No. CEC-500-04-073)*. California Climate Change Center.

Kirschbaum, M. U. F., & McMillan, A. M. S. (2018). Warming and elevated $CO_2$ have opposing influences on transpiration. Which is more important? *Current Forestry Reports*, *4*, 51–71. https://doi.org/10.1007/s40725-018-0073-8

Kunkel, K. E., Karl, T. R., Easterling, D. R., Redmond, K., Young, J., Yin, X., & Hennon, P. (2013). Probable maximum precipitation and climate change. *Geophysical Research Letters*, *40*, 1402–1408. https://doi.org/10.1002/grl.50334

Kusaka, H., & Kimura, F. (2004). Coupling a single-layer urban canopy model with a simple atmospheric model: Impact on urban heat island simulation for an idealized case. *Journal of the Meteorological Society of Japan*, *82*, 67–80. https://doi.org/10.2151/jmsj.82.67

Kusaka, H., Kondo, H., Kikegawa, Y., & Kimura, F. (2001). A simple single layer urban canopy model for atmospheric models: Comparison with multi-layer and slab models. *Boundary-Layer Meteorology*, *101*, 329–358. https://doi.org/10.1023/a:1019207923078

Littell, J. S., Peterson, D. L., Riley, K. L., Liu, Y., & Luce, C. H. (2016). A review of the relationships between drought and forest fire in the United States. *Global Change Biology*, *22*(7), 2353–2369. https://doi.org/10.1111/gcb.13275

Littell, J. S., McKenzie, D., Peterson, D. L., & Westerling, A. L. (2009). Climate and wildfire area burned in western U.S. ecoprovinces, 1916-2003. *Ecological Applications*, *19*(4), 1003–1021.

Litvak, E., McCarthy, H. R., & Pataki, D. E. (2017). A method for estimating transpiration of irrigated urban trees in California. *Landscape and Urban Planning*, *158*, 48–61. https://doi.org/10.1016/j.landurbplan.2016.09.021

Mann, M. E., & Gleick, P. H. (2015). Climate change and California drought in the 21st century. *Proceedings of the National Academy of Sciences of the United States of America*, *112*(13), 3858–3859. https://doi.org/10.1073/pnas.1503667112

Mesinger, F., DiMego, G., Kalnay, E., Mitchell, K., Shafran, P. C., Ebisuzaki, W., et al. (2006). North American regional reanalysis. *Bulletin of the American Meteorological Society*, *87*, 343–360. https://doi.org/10.1175/bams-87-3-343

Milly, P. C. D., Betancourt, J., Falkenmark, M., Hirsch, R. M., Kundzewicz, Z. W., Lettenmaier, D. P., & Stouffer, R. J. (2008). Stationarity is dead: Whither water management? *Science*, *319*, 573–574. https://doi.org/10.1126/science.1151915

Milly, P. C. D., & Dunne, K. A. (2017). A hydrologic drying bias in water-resource impact analyses of anthropogenic climate change. *Journal of the American Water Resources Association*, *53*, 822–838. https://doi.org/10.1111/1752-1688.12538

Miralles, D., van den Berg, M. J., Gash, J. H., Parinussa, R. M., de Jeu, R. A. M., Beck, H. E., et al. (2014). El Niño-La Niña cycle and recent trends in continental evaporation. *Nature Climate Change*, *4*, 122–126. https://doi.org/10.1038/nclimate2068

Mlawer, E. J., Taubman, S. J., Brown, P. D., Iacono, M. J., & Clough, S. A. (1997). Radiative transfer for inhomogeneous atmospheres: RRTM, a validated correlated-k model for the longwave. *Journal of Geophysical Research*, *102*, 16663–16682. https://doi.org/10.1029/97jd00237

Monin, A. S., & Obukhov, A. M. (1954). Basic laws of turbulent mixing in the surface layer of the atmosphere Contrib. *Proceedings of the USSR Academy of Sciences*, *151*, 163–187 (in Russian).

Monteith, J. L. (1995). A reinterpretation of stomatal responses to humidity. *Plant, Cell and Environment*, *18*, 357–364. https://doi.org/10.1111/j.1365-3040.1995.tb00371.x

Morrison, H., Thompson, G., & Tatarskii, V. (2009). Impact of cloud microphysics on the development of trailing stratiform precipitation in a simulated squall line: Comparison of one- and two-moment schemes. *Monthly Weather Review*, *137*, 991–1007. https://doi.org/10.1175/2008mwr2556.1

Mueller, B., Hirschi, M., Jimenez, C., Ciais, P., Dirmeyer, P. A., Dolman, A. J. et al. (2013). Benchmark products for land evapotranspiration: LandFlux-EVAL multi-data set synthesis. *Hydrology and Earth System Sciences*, *17*, 3707–3720.

Ozdogan, M., Rodell, M., Beaudoing, H. K., & Toll, D. L. (2010). Simulating the effects of irrigation over the United States in a land surface model based on satellite-derived agricultural data. *Journal of Hydrometeorology*, *11*, 171–184. https://doi.org/10.1175/2009JHM1116.1

Pall, P., Patricola, C. M., Wehner, M. F., Stone, D. A., Paciorek, C., & Collins, W. D. (2017). Diagnosing conditional anthropogenic contributions to heavy Colorado rainfall in September 2013. *Weather and Climate Extremes*, *17*, 1–6.

Pan, S., Tian, H., Dangal, S., Yang, Q., Yang, J., Lu, C., et al. (2015). Responses of global terrestrial evapotranspiration to climate change and increasing atmospheric $CO_2$ in the 21st century. *Earth's Future*, *3*, 15–35. https://doi.org/10.1002/2014EF000263

Patricola, C. M., & Wehner, M. F. (2018). Anthropogenic influences on major tropical cyclone events. *Nature*, *563*, 339–346. https://doi.org/10.1038/s41586-018-0673-2

Peterson, T. C., Golubev, V. S., & Groisman, P. Y. (1995). Evaporation losing its strength. *Nature*, *377*, 687–688. https://doi.org/10.1038/377687b0

Pierce, D. W., Cayan, D. R., & Dehann, L. (2016). *Creating climate projections to support the 4th California climate assessment*. Division of Climate, Atmospheric Sciences, and Physical Oceanography, Scripps Institution of Oceanography.

Qian, Y., Huang, M., Yang, B., & Berg, L. K. (2013). A modeling study of irrigation effects on surface fluxes and land-air-cloud interactions in the southern Great Plains. *Journal of Hydrometeorology*, *14*, 700–721. https://doi.org/10.1175/JHM-D-12-0134.1

Rasmussen, R., Liu, C., Ikeda, K., Gochis, D., Yates, D., Chen, F., et al. (2011). High-resolution coupled climate runoff simulations of seasonal snowfall over Colorado: A process study of current and warmer climate. *Journal of Climate*, *24*, 3015–3048. https://doi.org/10.1175/2010jcli3985.1

Roderick, M. L., Greve, P., & Farquhar, G. D. (2015). On the assessment of aridity with changes in atmospheric $CO_2$. *Water Resources Research*, *51*, 5450–5463. https://doi.org/10.1002/2015WR017031

Rodriguez Diaz, J. A., Weatherhead, E. K., Knox, J. W., & Camacho, E. (2007). Climate change impacts on irrigation water requirements in the Guadalquivir River basin in Spain. *Regional Environmental Change*, *7*, 149–159. https://doi.org/10.1007/s10113-007-0035-3

Romero-Lankao, P., Smith, J. B., Davidson, D. J., Diffenbaugh, N. S., Kinney, P. L., Kirshen, P., et al. (2014). North America. In V. R. Barros, C. B. Field, D. J. Dokken, M. D. Mastrandrea, K. J. Mach, T. E. Bilir, et al. (Eds.), *Climate change 2014: Impacts, adaptation, and vulnerability. Part B: Regional aspects. Contribution of working group II to the fifth assessment report of the intergovernmental panel on climate change* (pp. 1439–1498). Cambridge University Press.

Schär, C., Frei, C., Luthi, D., & Davies, H. C. (1996). Surrogate climate-change scenarios for regional climate models. *Geophysical Research Letters*, *23*, 669–672.

Seager, R., Hooks, A., Williams, A. P., Cook, B., Nakamura, J., & Henderson, N. (2015). Climatology, variability, and trends in the U.S. vapor pressure deficit, an important fire-related meteorological quantity. *Journal of Applied Meteorology and Climatology*, *54*(6), 1121–1141. https://doi.org/10.1175/jamc-d-14-0321.1

Shukla, S., Safeeq, M., AghaKouchak, A., Guan, K., & Funk, C. (2015). Temperature impacts on the water year 2014 drought in California. *Geophysical Research Letters*, *42*, 4384–4393. https://doi.org/10.1002/2015GL063666

Skamarock, W. C., & Klemp, J. B. (2008). A time-split nonhydrostatic atmospheric model for research and NWP applications. *Journal of Computational Physics*, *227*, 3465–3485. https://doi.org/10.1016/j.jcp.2007.01.037

Skamarock, W. C., Klemp, J. B., Dudhia, J., GillDO, B. D. M., Duda, M. G., et al. (2008). *A description of the advanced research WRF (Version 3 NCAR Technical Note NCAR/TN-475+STR)*. National Center for Atmospheric Research. https://doi.org/10.5065/D68S4MVH

Swann, A. L. S., Hoffman, F. M., Koven, C. D., & Randerson, J. T. (2016). Plant responses to increasing $CO_2$ reduce estimates of climate impacts on drought severity. *Proceedings of the National Academy of Sciences of the United States of America*, *113*, 10019–10024. https://doi.org/10.1073/pnas.1604581113

Trenberth, K. E., Jones, P. D., Ambenje, P., Bojariu, R., Easterling, D., Klein Tank, A., et al. (2007). Surface and atmospheric climate change. In S. Solomon, D. Qin, M. Manning, Z. Chen, M. Marquis, K. B. Averyt, et al. (Eds.), *Climate change 2007: The physical science basis. Contribution of working group I to the fourth assessment report of the intergovernmental panel on climate change* (pp. 235–336). Cambridge University Press.

US Census Bureau. (2014). State and County QuickFacts. Retrieved from https://www.census.gov/quickfacts

Vahmani, P., & Ban-Weiss, G. A. (2016). Impact of remotely sensed albedo and vegetation fraction on simulation of urban climate in WRF-urban canopy model: A case study of the urban heat island in Los Angeles. *Journal of Geophysical Research: Atmospheres*, *121*, 1511–1531. https://doi.org/10.1002/2015JD023718

Vahmani, P., & Hogue, T. (2014). Incorporating an urban irrigation module into the Noah Land surface model coupled with an urban canopy model. *Journal of Hydrometeorology*, *15*, 1440–1456. https://doi.org/10.1175/jhm-d-13-0121.1

Vahmani, P., & Hogue, T. S. (2015). Urban irrigation effects on WRF-UCM summertime forecast skill over the Los Angeles metropolitan area. *Journal of Geophysical Research: Atmospheres*, *120*, 9869–9881. https://doi.org/10.1002/2015jd023239

Vahmani, P., & Jones, A. D. (2017). Water conservation benefits of urban heat mitigation. *Nature Communications*, *8*, 1072. https://doi.org/10.1038/s41467-017-01346-1

Walton, D. B., Sun, F., Hall, A., & Capps, S. (2015). A hybrid dynamical-statistical downscaling technique: I. Development and validation of the technique. *Journal of Climate*, *28*, 4597–4617. https://doi.org/10.1175/jcli-d-14-00196.1

Wang, K., Dickinson, R., Wild, M., & Liang, S. (2010). Evidence for decadal variation in global terrestrial evapotranspiration between 1982 and 2002: 2. Results. *Journal of Geophysical Research*, *115*, D20113. https://doi.org/10.1029/2010JD013847

Wang, P., Li, D., Liao, W. L., Rigden, A. J., & Wang, W. (2019). Contrasting evaporative responses of ecosystems to heatwaves traced to the opposing roles of vapor pressure deficit and surface resistance. *Water Resources Research*, *55*, 4550–4563. https://doi.org/10.1029/2019WR024771

Wang, X., Zhang, J.-Y., Shahid, S., Guan, E.-H., Wu, Y.-X., Gao, J., & He, R.-M. (2016). Adaptation to climate change impacts on water demand. *Mitigation and Adaptation Strategies for Global Change*, *21*, 81–99. https://doi.org/10.1007/s11027-014-9571-6

Wickham, J. D., Stehman, S. V., Gass, L., Dewitz, J., Fry, J. A., & Wade, T. G. (2013). Accuracy assessment of NLCD 2006 land cover and impervious surface *Remote Sensing of Environment*, *130*, 294–304.

Williams, A. P., Seager, R., Abatzoglou, J. T., Cook, B. I., Smerdon, J. E., & Cook, E. R. (2015). Contribution of anthropogenic warming to California drought during 2012–2014. *Geophysical Research Letters*, *42*, 6819–6828. https://doi.org/10.1002/2015GL064924

Yang, Y., Roderick, M. L., Zhang, S., McVicar, T. R., & Donohue, R. J. (2019). Hydrologic implications of vegetation response to elevated $CO_2$ in climate projections. *Nature Climate Change*, *9*, 44–48. https://doi.org/10.1038/s41558-018-0361-0

Yang, Z., Dominguez, F., Zeng, X., Hu, H., Gupta, H., & Yang, B. (2017). Impact of irrigation over the California Central Valley on regional climate. *Journal of Hydrometeorology*, *18*, 1341–1357. https://doi.org/10.1175/JHM-D-16-0158.1